Hydrogen Production with Seawater-Resilient Bipolar-Membrane Electrolyzers

Daniela H. Marin,[1,2,†] Joseph T. Perryman,[1,2,†] McKenzie A. Hubert,[1,2] Grace A. Lindquist,[3] Lihaokun Chen,[3] Ashton M. Aleman,[1,2] Gaurav A. Kamat,[1,2] Valerie A. Niemann,[1,2] Michaela Burke Stevens,[2] Yagya N. Regmi,[4] Shannon W. Boettcher,[3,*] Adam C. Nielander,[2,**] Thomas F. Jaramillo,[1,2,5,***]

[1]Department of Chemical Engineering, Stanford University, Stanford, CA 94305

[2]SUNCAT Center for Interface Science and Catalysis, SLAC National Accelerator Laboratory, Menlo Park, CA 94025

[3]The Department of Chemistry and Biochemistry and the Oregon Center for Electrochemistry, Eugene, OR 97403

[4]Manchester Fuel Cell Innovation Centre, Department of Natural Sciences, Manchester Metropolitan University, Manchester, UK

[5]Lead Contact

† These Authors Contributed Equally

*Correspondence: swb@uoregon.edu

**Correspondence: anieland@slac.stanford.edu

***Correspondence: jaramillo@stanford.edu

SUMMARY

Generation of H_2 and O_2 from untreated water sources represents a promising alternative to ultrapure water required in contemporary proton exchange membrane-based electrolysis. Bipolar membrane-based devices, often used in electrodialysis and CO_2 electrolysis, facilitate impure water electrolysis via simultaneous mediation of ion transport and enforcement of advantageous microenvironments. Herein we report their application in direct seawater electrolysis; we show that upon introduction of ionic species such as Na^+ and Cl^-, bipolar membrane electrolyzers inhibit the oxidation of Cl^- to corrosive OCl^- at the anode from real seawater down to a Faradaic efficiency of 0.005% while proton exchange membrane electrolyzers under comparable operating conditions exhibit a 10% Faradaic efficiency to Cl^- oxidation. The effective mitigation of Cl^- oxidation by bipolar membrane electrolyzers underpins their ability to enable longer term seawater electrolysis than proton exchange membrane assemblies by a factor of 140, suggesting a path to durable seawater electrolysis.

Up to 10 keywords may be included here. (Please note that keywords are not carried over from the editorial submission system.) Seawater, electrolysis, bipolar membranes, chloride oxidation, saline, anon exchange membrane, proton exchange membrane,

INTRODUCTION

Sustainable generation of chemical fuels such as H_2 offers a means to address the long-duration energy-storage challenge and to enable a next-generation, carbon-neutral chemical industry.[1] To this end, low-temperature water electrolysis driven by renewable electricity is a promising route to inexpensive, sustainably produced H_2 that does not generate greenhouse gas emissions. While traditional membrane electrolyzers rely on ultrapure water feeds to generate H_2 and O_2, the direct electrolysis of impure water sources, e.g. seawater, could have inherent advantages, enabling broader access to water feedstocks while reducing capital costs by mitigating the need for on-site water purification.[2–6] However, electrolyzing seawater to generate H_2 and O_2 introduces distinct challenges in comparison to electrolyzing ultrapure water. One critical challenge arises from the high concentrations of ionic species (e.g., Cl^-, Na^+, SO_4^{2-}, Mg^{2+}, Ca^{2+}, etc.) — particularly Cl^- — in seawater. The Cl^- oxidation reaction (COR) generates corrosive 'free chlorine' species (i.e., Cl_2, HOCl, OCl^-) at the electrolyzer anode. While the electrooxidation of Cl^- to Cl_2 (ie the chlorine evolution reaction—ClER) is a critical industrial process (e.g., chlor-alkali process),[7] COR poses significant challenges to the safety, efficiency, and durability of seawater electrolyzers during operation.[8–12] Mitigating the COR

with impure water feed also opens the possibility of making use of a pure O_2 stream from the anode for uses including undersea operations and life-support.

The COR reaction can, in principle, be suppressed by ***i***) decreasing anode catalyst selectivity for the COR, ***ii***) modifying the anodic microenvironment to disfavor Cl^- oxidation and/or ***iii***) decreasing Cl^- access to the anode.[12–15] Developing catalysts that strongly favor the 4-electron oxygen evolution reaction (OER) over the 2-electron COR at relevant applied potentials is an active area of research.[16,17] IrO_x is an efficient precious-metal OER catalyst in Cl^--free electrolyte, but in electrolytes with Cl^- at concentrations as low as ~30 mM yields a high COR Faradaic efficiency of ~86%.[18] Non-precious metal oxide catalysts, such as MnO_x, have shown promising OER selectivity (93%) in these same low-Cl^- concentration electrolytes, but material stability challenges in acidic pH are not yet resolved.[19,20] Strategies (***ii***) and (***iii***) are complementary and leverage device architectures to create local electrolyte conditions that disfavor COR, for example by creating an alkaline anode environment where the oxidation of Cl^- is disfavored thermodynamically with respect to OER,[17,21] or by selectively inhibiting the transport of Cl^- to the anode, for example using cation-selective membranes.

Here we demonstrate how strategies (***ii***) and ***(iii)*** enabled near complete suppression of Cl^- oxidation even with a seawater feed. Our approach uses a bipolar membrane (BPM), composed of a cation exchange layer (CEL) combined with an anion exchange layer (AEL) integrated into a bipolar membrane water electrolyzer (BPMWE) device.[22–24] We found that an appropriately designed BPMWE, in concert with an asymmetric electrolyte feed in which seawater is only present at the cathode, mutually captured both the advantages of the CEL that limits Cl^- crossover to the anode (due to cation transport selectivity), and the AEL that provides a local alkaline anode pH (where OER catalysts have high selectivity and mitigate the COR), resulting in an inherently ion-tolerant seawater electrolyzer (**Figure 1A**). We evaluated the ion-transport properties, performance, selectivity, and durability of the BPMWEs with saline water feeds and compared them to monopolar proton exchange membrane water electrolyzers (PEMWEs). We demonstrated BPMWE devices operating with real seawater — collected from the Pacific Ocean (Half Moon Bay, CA, USA) — in the cathode feed, as well as in both electrode feeds, during sustained direct seawater electrolysis to generate H_2 and O_2 at current densities reaching 250 mA cm^{-2}.

RESULTS AND DISCUSSION

BPMWE and PEMWE architectures were fabricated according to the designs in **Figure 1** and **Figure S1** Extended descriptions of the experimental fabrication and electrochemical methods are provided in the Methods section and in the SI. AEMWEs (anion exchange membrane water electrolyzers) were similarly fabricated, but significant Cl^- crossover precluded robust comparison to BPMWE and PEMWE (see **Figure S2**). While the AEMWE is not examined in detail in the present work owing to its inability to circumvent anion crossover and subsequently maintain favorable anode pH over time, it should be noted that, similar to the case of the BPMWE, thermodynamic analysis suggests that an AEMWE could be expected to operate without generating significant corrosive species and may also represent an alternative to the PEMWE architecture under conditions in which the AEMWE is durable to local pH changes.

Electrolysis in Deionized Water and 0.5 M $NaCl_{aq}$

We characterized the *j-V* behavior of BPMWEs compared to PEMWEs under two different water feed conditions: a 'symmetric' (same feed composition fed to each electrode) DI-water condition and an 'asymmetric' (different feed composition fed to each electrode) saline condition. In the 'symmetric' DI-water condition, high-purity deionized water (18.2 MΩ cm) was circulated through both the anode and the cathode chambers (**Figure 1A** and **1B**). In the 'asymmetric' saline condition, we simulated seawater using 0.5 M $NaCl_{aq}$, which approximates the ~0.55 M Cl^- and ~0.47 M Na^+ concentrations in seawater,[25] and was fed to the cathode chamber while DI water was fed to the anode chamber. This asymmetric condition mimicked the conditions of an electrolyzer operating with seawater fed only to the cathode and facilitated measurements of ion crossover (Cl^-/Na^+) and Cl^- oxidation behavior (see below).

Using symmetric DI water feeds, the voltage required to operate the PEMWE was 60 mV less than the BPMWE at j = 50 mA cm^{-2}, increasing to a voltage difference of 670 mV at j = 500 mA cm^{-2} (**Figure 2A** and **2B** and **Table 1**). The voltage differences between the two devices is broadly consistent with recent reports on state-of-the-art performance for PEMWEs and BPMWEs.[26,27] the difference is attributed to the energy input required to drive

water dissociation (WD, $H_2O \rightarrow H^+ + OH^-$) at the CEL/AEL junction of the BPMWE, as well as the superior performance of Nafion proton exchange ionomer in comparison to PiperION-A40 anion exchange ionomer—this has been highlighted in recent work that highlighted that AEL ionomers are more susceptible to oxidative degradation mechanisms than CEL ionomers.[10, 25-28]

For both the PEMWE and BPMWE, using 0.5 M $NaCl_{aq}$ as the cathode feed (**Figure 2A** and **2B**) increased total cell voltage with respect to the symmetric DI water-fed conditions (**Table 1**). We hypothesize that a significant fraction of the PEMWE/BPMWE performance loss reflects decreased $[H^+]$ at the cathode-CEL interface due to exchange between Na^+ and H^+ in the initially protonated CEL.[28] We interpret the transient voltage spikes seen in **Figure 2C**, which are only observed as the applied current density was changed in the presence of 0.5 M $NaCl_{aq}$, to be a result of a changing steady-state $[Na^+]$ and $[H^+]$ at the cathode-CEL interface; these concentration changes are likely due to shifts in the balance between diffusion and migration of both cations. As current density increases, H^+ migration toward the cathode-CEL interface increases relative to Na^+ diffusion into the same interface, leading to a decrease in voltage over time owing to a progressively more protonated CEL. The reverse is true when decreasing the current density, which results in a progressively less protonated, more sodiated cathode-CEL interface. Hence, a steady-state $[H^+]$ at the cathode-CEL interface reflects balance between multiple transport processes—including diffusion of Na^+ from the bulk solution toward the cathode-CEL interface and migration of H^+ generated at the anode or WD layer toward the cathode (discussed below). The generation of local pH gradients over time between the anode and cathode in these systems may also contribute to observable changes in cell voltage owing to the decrease in reactant (i.e., H+, OH-) concentration — direct measurements of local pH at the electrode-electrolyte interface are the target of future work.

The BPMWE cell voltage was more affected by the addition of NaCl to the feed at 500 mA cm^{-2} than the PEMWE cell voltage (ΔV_{BPMWE} = 0.9 V; ΔV_{PEMWE} = 0.41 V). We assigned this difference to losses associated with water dissociation and/or the AEL-anode catalyst interface of the BPMWE, as the cathode catalyst environments are identical in both electrolyzers. Impedance analysis (**Figure S3-S9**) suggests that the additional performance losses for the BPMWE can be attributed in part to increased water dissociation resistance ($\Delta R_{WD,500\ mA}$ = 33 mΩ) in the BPMWE upon the addition of NaCl, along with higher series resistance ($\Delta R_{s,500\ mA}$ = 249 mΩ) compared to the PEMWE ($\Delta R_{s,\ 500\ mA}$ = 43 mΩ) (**Figure S9**). As anion-exchange polymers generally demonstrate lower ionic conductivity due to the intrinsic lower mobility of OH^- relative to H^+ in cation-exchange polymers,[29] we expect conductivity losses from competing OH^-/Cl^- transport in the AEL will have a larger effect on performance relative to competing H^+/Na^+ transport in the CEL. Thus, we attribute the increased series resistance to a decrease in OH^- conductivity in the AEL as well as in the ionomer in the catalyst layer.[30] Cl^- or Na^+ ions that reach the BPM junction might also block WD catalyst active sites, contributing to the increase in R_{WD}. Although, careful selection of membranes, operating conditions, and catalyst identity are all potential routes to mitigating WD catalyst poisoning.

Ion Crossover Dynamics

To probe the ion-transport mechanisms that underpin PEMWE and BPMWE operation under saline conditions, we evaluated both electrolyzer architectures in the asymmetric saline electrolyte feed mode. **Figure 3A** and **Figure 3B** depict the rate of Cl^- and Na^+ transport, respectively, from the cathode to anode chambers for both BPMWEs and PEMWEs with 0.5 M $NaCl_{aq}$ circulating at the cathode and DI water at the anode. In the absence of an applied current, there was no statistical difference in the rate of Na^+ and Cl^- crossover, consistent with the electroneutrality requirements that Na^+ and Cl^- move through the membrane together.[31] Upon application of current, Na^+ transport is significantly suppressed, decreasing by ~3x in the PEMWE and ~13x in the BPMWE. The decreased Na^+ transport rate is consistent with the direction of the applied voltage driving positively charged species from the anode to the cathode. We ascribe the additional decrease in Na^+ crossover rate in the BPM to the AEL further blocking cation movement by Donnan exclusion (**Figure 3C**). Conversely, applied current did not have a significant influence on Cl^- transport (**Figure 3A**). The low, non-zero crossover rate of Cl^- for both the BPMWE and PEMWE is consistent with a Donnan exclusion effect at the cathode/CEL interface (**Figure 3C**) that limits the crossover of negatively charged species despite a large concentration gradient in Cl^- between the cathode and anode feeds (~5 M_{Cl^-} mm^{-1}) favoring diffusive Cl^- crossover.[32] The similarity in Cl^- ion flux across the BPMWE and PEMWE regardless of current density ($J^{Cl^-}_{avg,BPMWE}$ = 7.5 × 10^{-9} M cm^{-2} s^{-1} and $J^{Cl^-}_{avg,PEMWE}$

= 8.0 × 10^{-9} M cm^{-2} s^{-1}) suggests that the AEL does not modulate anion crossover rates, though it may offer important advantages when a wider array of ions (e.g. K^+, Mg^{2+}, Ca^{2+}) are present (e.g., real seawater feed). Based on the low Cl^- transport rates observed, the percent of current carried by Cl^- crossover was low (~1%) at low applied current densities (e.g., j = 50 mA cm^{-2}), and decreases to < 0.1% with increased applied current densities for both the BPMWE and PEMWE (see SI and **Figure S10**).[33] Increasing the applied current density from j = 50 mA cm^{-2} up to j = 500 mA cm^{-2} did not have a further inhibitory effect on the Na^+ crossover rate nor a clear promoting effect on the Cl^- crossover rate. This suggests there may be some mechanism(s) beyond transport via migration influencing ion crossover rates, such as current-dependent membrane-transport selectivity effects (i.e. preferential acceleration of more-mobile H^+ or OH^- transport rather than less mobile Na^+ or Cl^- transport or other concentrated electrolyte effects).[34]

The ion crossover data shows that the BPMWE inhibits Na^+ crossover while both the BPMWE and PEMWE inhibit Cl^- transport. Neither Na^+ nor Cl^- transport was significantly affected by increasing migration driving forces suggesting that migration forces are not the sole driver of the observed ion transport phenomenon. This discrepancy may highlight competition with vehicular and/or Grotthuss transport of H^+ and OH^- through the CEL and AEL, respectively.[35] In any case, however, the total charge carried via Cl^- migration is very low for both membrane architectures, capturing the advantage of the CEL in limiting Cl^- crossover and thereby inhibiting COR at the anode under asymmetric electrolyte conditions.

Cl^- Electrooxidation

Under asymmetric 0.5 M $NaCl_{aq}$ feed conditions, only Cl^- which crossed from cathode to anode should be available for oxidation to free chlorine products. We measured a maximum Faradaic efficiency *FE* = 0.095% for COR at j = 100 mA cm^{-2} in the PEMWE while we measured FE = 0.001% to COR for the BPMWE (**Figure 4**).

Corrosive free chlorine species are known to spontaneously degrade over time due to several factors: temperature, light, pH, and ionic strength of the solution.[36] We found the rate of free chlorine loss in both devices would be nearly identical if present in equal concentrations (**Figure S11**), excluding the possibility that differential free-chlorine degradation rates explain the differences in COR *FE* despite the similarity of $j_{\mathrm{avg}}^{\mathrm{Cl}^-}$ in both electrolyzers. Owing to the interesting trend in COR behavior observed for the PEMWE compared to the BPMWE as shown in **Figure 4**, we also analyzed the COR in three-electrode H-cells with 0.5 M $NaCl_{aq}$ as the electrolyte at both 100 mA cm^{-2} and 250 mA cm^{-2}. In these experiments, we observed a *FE* of 4.0% at 100 mA cm^{-2} and 1.1% at 250 mA cm^{-2} in the acidic simulated PEMWE anode microenvironment, compared with <0.01% in the alkaline simulated BPMWE anode microenvironment (**Figure S12**) at both current densities. This data is in good agreement with the trend that COR *FE* actually decreases at current densities beyond 100 mA cm^{-2}, and further indicates that the low local pH of the PEMWE promotes COR while the higher pH present in the BPMWE anode microenvironment suppresses the generation of corrosive free chlorine species — this is consistent with more favorable thermodynamics at increasing pH for OER relative to COR (**Figure S13**).[21] We also found the simulated PEMWE anode selectivity for COR decreased from 4.0% to 1.1% from 100 mA cm^{-2} to 250 mA cm^{-2}, consistent with the lower fraction of the current carried by Cl^- at higher current density **(Figure S10**).

Electrolyzer Stability with 0.5 M $NaCl_{aq}$ and Seawater

Under galvanostatic conditions with asymmetric 0.5 M $NaCl_{aq}$ feed conditions, both the BPMWE and PEMWE demonstrated cell voltage degradation rates over 6 hours ($\Delta V_{6\,h}$) below 50 mV h^{-1} for a range of current densities. The BPMWE showed a smaller average voltage degradation rate than the PEMWE at all current densities except 500 mA cm^{-2} (**Figure S14**). However, the standard deviation in the measurements (**Figure S15**, **Table S1**) precluded our ability to determine with sufficient confidence that either electrolyzer voltage was more stable over 6 hrs of asymmetric 0.5 M NaCl electrolysis. Building on the promising results observed for electrolyzers operating under asymmetric saline feed conditions, we evaluated the performance of BPMWEs and PEMWEs operating with 0.5 M $NaCl_{aq}$ and real seawater acquired from Half Moon Bay, CA. **Figure 5A** shows the observed cell voltage for both electrolyzer architectures operating at 250 mA cm^{-2} upon introduction of seawater to their cathode feeds. Here, the increase in total cell voltage was 0.84 V in the BPMWE—slightly higher than the increase of 0.75 V with 0.5 M $NaCl_{aq}$. Similarly, the increase in seawater-fed cell voltage for the PEMWE was 0.82 V, compared to 0.41 V with 0.5 M $NaCl_{aq}$. These results highlight the additional voltage sensitivity for both electrolyzer architectures, but particularly

for the PEMWE, to the presence of the other mono-, di-, and tri-valent ionic constituents present in real seawater.

For the first 6 h, the stability of a BPMWE with seawater as the cathode feed was within experimental error to a BPMWE fed with 0.5 M $NaCl_{aq}$ (**Figure 5A, S15**). The seawater-fed electrolysis experiments demonstrated $\Delta V_{6\,h}^{BPM}$ = 29 ± 20 mV h^{-1} over 6 h, as compared to 28 ± 8 mV h^{-1} for 0.5 M $NaCl_{aq}$ experiments (**Figure S14-S15**) and ~15 mV h^{-1} for state-of-the-art BPMWEs operating in symmetric DI water fed conditions.[27] In DI water, the voltage loss over time is attributed to anion exchange polymer degradation.[37,38] Analysis of the bulk cathode and anode feed pH changes over time in real seawater electrolysis experiments (**Figure S16**) reveal that performance losses may be correlated with increasing pH gradients across the device, giving rise to potential losses.[39] After >100 h of continuous BPMWE operation at 250 mA cm^{-2}, free chlorine had only formed with a Faradaic efficiency of 0.005% and is therefore not believed to contribute to the observed voltage degradation rate. Under the same asymmetric seawater conditions, the PEMWE failed after ~50 h and had rapidly generated more free chlorine (~ 20μM) in the first 24 h of operation than the BPMWE had over the course of >100 h operation. This accelerated PEMWE voltage degradation is consistent with our observation that formation of corrosive free chorine reduces device longevity (**Figure S17**). Although the BPMWE cell voltage was more sensitive than the PEMWE cell voltage to the inclusion of the 0.5 M NaCl in the cathode feed (**Table 1**), we believe that the extended electrolysis time of the asymmetric seawater experiments accentuated the difference cell voltage stability engendered by differential production of free chlorine in the PEMWE versus the BPMWE.

When seawater was introduced to both the cathode feed *and* the anode feed, the increase in total cell voltage was 0.90 V for the BPMWE. No voltage spike could be clearly quantified for the PEMWE upon addition of real seawater to its feeds because the voltage rapidly increased until failure within 3 min of operation (**Figure 5B**), likely due to the generation of corrosive free chlorine species at its acidic anode-CEL environment. After 3 min of electrolysis with seawater fed to both the anode and cathode, COR *FE* was 10% for the PEMWE, while the BPMWE did not generate any detectable free chlorine species throughout 7 h of direct, unprocessed seawater electrolysis. Post-experiment analysis (**Figures S18-S22**), suggests precipitation of divalent cation hydroxides—predominately of $Mg(OH)_2$—as a significant additional contributor to performance loss in real seawater for both architectures, as has been discussed in previous work.[15] Additional post-experiment ICP-MS analysis is presented in **Table S2** and **Table S3**, illustrating relatively low levels of Ir and Pt loss from the anode of each electrolyzer.

Conclusions

We designed, fabricated, and evaluated PEMWEs and BPMWEs operating under asymmetric and symmetric saline electrolyte conditions to generate H_2 and O_2 at high current densities for extended periods of time. We quantified the effect of feed contamination on performance in terms of energy efficiency and device durability, charting a new path and design principles for deployable, durable, and efficient direct electrolysis of impure water.

Despite higher operating voltages than PEMWEs, BPMWEs uniquely mitigate undesired ion transport (e.g. Cl^- crossover in this case) and control selectivity for O_2 production in high-salinity testing conditions. We propose that Na^+ transport in/through the protonated Nafion ionomer of both electrolyzers, however, likely reduces the H^+ concentration at the cathode, slowing HER kinetics, illustrating the need for microenvironment design at the electrode interfaces. Interestingly, the partial currents of Na^+ and Cl^- that cross the BPM were largely independent of cell voltage and (total) current density, suggesting more-complex interactions beyond standard dilute electrolyte theory and motivating additional work to understand operative transport dynamics in impure water electrolyzers and other electrochemical technologies. The BPMWE also provides a locally basic pH at the anode and thus inhibits the generation of corrosive free chlorine that is formed in the acidic PEMWE anode and leads to rapid PEMWE failure in seawater.

The robust zero-gap BPM seawater electrolyzer reported here operated at current densities of 250 mA cm^{-2} and serves as a benchmark for membrane electrolyzer durability with impure feeds, providing a unique route to avoid Cl^- oxidation, increase efficiency, and prevent device failure without requiring ultrapure water. Despite significant improvements in durability for the BPMWE compared to the PEMWE, decreased voltage stability for both systems fed with seawater indicates that other failure mechanisms arise from the more complex electrolyte composition. As such, deployment of these devices still requires

significant improvements in cell voltage and durability; >50,000 h lifetimes and cell voltage degradation rates between 10-20 μV h^{-1} are common in commercial (pure water) electrolyzers.[40–43] To this end, device components such as membranes, PTLs, flow-fields, and catalysts all remain viable targets for improving performance and durability for seawater electrolysis.[10,44]

EXPERIMENTAL PROCEDURES

Resource Availability

Lead Contact

Further information and requests for resources should be directed to and will be fulfilled by the Lead Contact, Thomas F. Jaramillo, at jaramillo@stanford.edu.

Materials Availability

This study did not generate new unique reagents.

Data and Code Availability

The data generated during this study are available upon request to jaramillo@stanford.edu.

Materials

Electrodes and membranes were prepared according to recent reports.[27] NaCl (99.0% trace metals basis) was used as purchased from Sigma Aldrich in all saline water (0.5 M $NaCl_{aq}$ experiments. Cationic impurities of NaCl include Ca^{2+} (< 0.002%), Mg^{2+} (< 0.001%), K^{+} (<0.005%) and Fe $^{2+/3+}$ (< 2 ppm). Here, deionized water (DI) refers to ultra-pure deionized water with a measured resistivity of approximately 18.2 MΩ·cm. Nafion 212 and PiperION-A40 membranes and ionomers were used as the cation- and anion-selective layers (CEL and AEL), respectively, in the BPMWE. The BPMWE anode consisted of IrO_x nanoparticles (5-10 nm dia.) on a stainless-steel porous transport layer (PTL) while the PEMWE integrated the same IrO_x nanoparticles onto a platinized titanium PTL. The cathode in both electrolyzers was Pt black (34 $m^2 g^{-1}$) deposited on Toray carbon paper PTL.

Anode Preparation

Anodes for BPMWE and PEMWE devices were fabricated by preparing a catalyst ink and then spraying the ink onto a porous transport layer (PTL) substrate. To produce the ink, iridium oxide (0.1 g) [Fuel Cell Store], ultrapure deionized water (0.5 g, 18.2 MΩ·cm), isopropyl alcohol (1.7 g), and 5%wt ionomer (BPMWE: PiperION (0.1 g) [Versogen]; PEMWE: Nafion 212 (0.1 g) [Sigma Aldrich]) were, in that order, added to a 20 mL glass scintillation vial. The vial was bath sonicated for 10-20 minutes or until the ink mixture was evenly dispersed. A 5 cm x 5 cm PTL substrate (BPMWE: stainless steel, 25AL3 [Bekaert Bekipor®]; PEMWE: platinized titanium fiber felt, [Fuel Cell Store]) was prepared and the back of the layer was pencil traced with gridlines of a 4 cm x 4 cm square and weighed. The front of the PTL was framed with tape to make a 4 cm x 4 cm spray area and then placed onto a hotplate (100 °C). Using a hand-held airbrush [Testors], the catalyst ink was sprayed perpendicular to the hotplate in a pulsed serpentine pattern (8-12psi) until the catalyst reached the desired loading (2.5 mg cm^{-2} | 40 mg total). The surface was allowed to evaporate before spraying a new layer of catalyst by waiting about 5 s between each serpentine pattern. To weigh the catalyst mass between sprays, the tape frame was removed, and the electrodes were allowed to cool to room temperature before weighing. A new tape frame was placed around the active spray area. After the catalyst was sprayed, dilute ionomer solution (BPMWE: 2% PiperION; PEMWE: 5% Nafion) solution in ethanol was sprayed over the catalyst layer in a pulsed serpentine pattern until the ionomer overlayer reached 10-20% of the catalyst mass weight (4-8 mg). The anodes were stored in a polystyrene container at room temperature until use.

Cathode Preparation

Cathodes for the PEMWE and BPMWE were fabricated identically by preparing a catalyst ink and subsequently spraying the ink onto a carbon-based PTL. In detail, platinum catalyst (0.1g) [Fuel Cell Store], ultrapure deionized water (1.5 g, 18.2 MΩ·cm), isopropyl alcohol (1.7g), and 5%wt Nafion (0.1g), in that order, were added to a 20 mL glass scintillation vial. The vial was bath sonicated for 20-30 minutes or until the ink mixture was evenly dispersed. If the ink was not fully dispersed, the bath sonication was followed with 20 s of probe sonication pulses with 5 second rest for 1.5 minutes. A 5 cm x 5 cm Toray carbon PTL was cut, and the back of the layer was pencil traced with gridlines of a 4 cm x 4 cm square and weighed. The front of the

PTL was framed with tape to make a 4 cm x 4 cm spray area and then placed onto a hotplate (100 °C). Using a hand-held airbrush [Testors], the catalyst ink was sprayed perpendicular to the hotplate in a pulsed serpentine pattern (8-12psi) until the catalyst reached the desired loading (2 mg cm^{-2} | 32 mg total). The surface was allowed to evaporate before spraying a new layer of catalyst by waiting about 5 s between each serpentine pattern. To weigh the catalyst mass between sprays, the tape frame was removed, and the electrodes were allowed to cool to room temperature before weighing. A new tape frame was placed around the active spray area. After the catalyst was sprayed, a 5% Nafion solution was sprayed over the catalyst layer in a pulsed serpentine pattern until the ionomer overlayer reached 10-20% of the catalyst mass weight (3.2-6.4 mg). The cathodes were stored in a polystyrene container at room temperature until use.

Bipolar Membrane Preparation

Bipolar membranes were prepared using a Nafion 212 (50.8 µm) [Fuel Cell Store] proton exchange membrane and ionomer as the CEL, PiperION TP-85 (40 µm) [Versogen] anion exchange membrane and ionomer as the AEL, and a TiO_2 nanoparticulate water dissociation catalyst layer. TiO_2 nanoparticles (0.1 g) [Nippon Aerosil Co., Ltd] were dispersed in water (4.9 g). The ink was sonicated for 5 minutes. A small amount of this concentrated TiO_2-water "mother ink" (30 mg) was diluted in a water and IPA (2-propanol) mixture (0.47 g water, 1.7 g IPA). The diluted ink was bath sonicated for 5 minutes prior to spraying. The as-received Nafion membrane was removed from the plastic backing and soaked in DI water over night. The edges of the Nafion membrane (cut with scissors to 1.5 cm x 1.5 cm) was carefully taped onto a glass petri dish ensuring no air bubbles present, leaving a 1.2 cm x 1.2 cm area exposed, and the petri dish was laid flat on a hot plate (90 °C) in a fume hood. The diluted TiO_2 ink was then hand-sprayed ([Testors], ~45° incident angle to the hot plate surface, 15 psi) onto the Nafion membrane in bursts (~1 s). The burst pattern involved spraying 10 times, then rotating the sample 90° and repeating until the ink was completely used. The air flow from the fume hood and spray methodology were important in reproducing the TiO_2 loading and morphology on the Nafion membrane. When the entirety of the dilute TiO_2 ink was sprayed, the tape was carefully removed from the edges of the membrane, using water to help lift the tape. The edge of the membrane was marked to identify what side had been sprayed, and the membrane was stored in DI water until ready to assemble the electrolyzer, when it was combined with the PiperION anion exchange membrane.

Seawater Treatment

Seawater was collected from Half Moon Bay, CA and filtered to remove suspended solids prior to incorporation into either electrolyzer reservoir during testing. This simple filtration mitigated potential clogging of the diaphragm pumps by particulate matter during long-term circulation of the seawater.

Electrolyzer Assembly

Commercial electrolyzer hardware (5 cm^2, [Fuel Cell Technologies, Inc.]) was used in all tests, in configurations shown in **Figure 1**. A Ti flow field was used for the anode side, and a graphite flow field was used for the cathode side. Assembling from the anode side, gaskets (polyethylene terephthalate (PETE), 0.047" for BPMWE, 0.037" for PEMWE, cut with a 1 cm x 1 cm opening) were stacked on top of the titanium flow field. A porous Ti support was placed in the gasket opening followed by the anode porous transport layer, catalyst side up. The PiperION membrane (1.5 x 1.5 cm) was placed on top of the PTL. The TiO_2-coated Nafion membrane was placed on top of the PiperION membrane, with the TiO_2 side facing down (towards the PiperION). Additional gaskets were placed on top (PETE, 0.037" cut with a 1 cm x 1 cm opening) and the cathode PTL was placed in the gaskets, catalyst side down (facing the Nafion membrane). A Ti support was placed on top of the cathode PTL. The cathode flow field, current collector, and back plate were placed on top. The hardware was tightened to 50 lbs-in (5.65 N-m).

Electrolyte Flow Conditions

The electrolyzer was connected to two separate water re-circulating loops — one for the cathode and one for the anode. Each loop circulated to and from their own respective 1 L reservoirs of water heated to 60 °C. The water was supplied to both the anode and cathode with a calibrated flow of 60 mL/min. Electrochemical measurements began when the cell temperature, as measured by a K-type thermocouple at the cathode back plate, reached 50

°C (+/- 1 °C), which took ~30 min for each experiment. The cell temperature was maintained at 50 °C (+/- 1 °C) by tuning the water temperature in the reservoirs as appropriate.

Electrolyzer Break-In and Operation

A break-in procedure was performed before each experiment, with DI water circulating to both cathode and anode electrolyzer compartments. First, current was held at 10 mA for 1 min. The current was then sequentially stepped up in 50 mA increments from 50 mA to 500 mA, holding each current for 1 min prior to stepping to the next. In the final increment, current was held at 500 mA for a total of 10 min, at which point a "break-in potential" was recorded to ensure that baseline device performance was as expected. If the break-in voltage of a BPM was >2.5 V or of a PEM was >1.9 V at 500 mA cm^{-2}, the electrolyzer was disassembled and reassembled with a new membrane electrode assembly (MEA). This first sequence is coined as "CP1" and can be seen for all three membrane architectures in **Figure S2A** and **Figure S2B**. Following this increasing first sequence of stepped chronopotentiometry, the current was stepped back down in 50 mA increments from 500 mA to 50 mA, again holding each current for 1 min, followed by 1 min at 10 mA. This decreasing sequence of stepped chronopotentiometry is coined as "CP2". Next, a rapid, increasing stepped chronopotentiometry sequence was performed starting at 10 mA for 10 s, and then again stepping the current in 50 mA increments from 50 mA to 500 mA holding each for 10 s. This last sequence is coined as "CP3". Polarization curves shown in **Figure 2A-B** were extracted from stabilized voltages at the end of each current step in CP1, prior to increasing applied current density. This method avoids spurious results that might otherwise arise from extracting voltages at non-steady state membrane conditions.

Following the completion of CP3, a series of galvanostatic electrochemical impedance spectroscopy (GEIS) scans were performed at fixed current densities of 500 mA cm^{-2} (GEIS 4), 250 mA cm^{-2} (GEIS 5), 100 mA cm^{-2} (GEIS 6), 50 mA cm^{-2} (GEIS 7), and then at the target current density for long-term electrolysis (GEIS 8), with superimposed AC currents having magnitudes of 10% of each respective DC current. AC oscillation frequencies were scanned from 200 kHz to 20 mHz to extract circuit resistances, voltage-dependent charge-transfer resistances, and voltage-dependent water-dissociation resistances (in the case of a BPM) prior to the addition of simulated (0.5 M $NaCl_{aq}$) or real seawater.

After the break-in procedure, the current was held constant at either 0, 50, 100, 250, or 500 mA for 6 hr. When the voltage reached a steady-state value (~5 min), either NaCl (29.22 g) was added to the cathode reservoir (1 L) to create a 0.5 M $NaCl_{aq}$ cathode feed solution, or pre-heated seawater from Half Moon Bay, CA was exchanged as the cathode feed solution, depending on the desired experiment. An aliquot of 5 mL was taken for inductively coupled plasma mass spectrometry (ICP-MS) analysis (ThermoScientific iCAP RQ)and pH measurements (accumet BASIC, accuTupH probe) from the anode feed at t = 0 s (immediately before the salt was added), 1 hr, 3 hr, and 6 hr. Aliquots of 10mL were also taken from the anode feed for additional analysis via UV-Vis to quantify free chlorine concentrations at elapsed times of 1, 3 and 6 hours after the addition of NaCl. Throughout this constant current experiment, additional GEIS experiments were performed at the same current density (GEIS 10-16) to monitor changing impedance over time.

Inductively Coupled Plasma Mass-Spectrometry Measurements

Trace element analysis (**Table S2** and **Table S3**) was performed with ICP-MS (ThermoFisher Scientific, iCAP RQ) using a parallel flow nebulizer (Burgener PEEK Mira Mist) and a Peltier-cooled Scott-type double-pass cyclonic spray chamber cooled to 2.7 °C. Forward radio frequency plasma generator power was set to 1550 W with argon flows of 14 L min^{-1} for carrier gas, 0.8 L min^{-1} for cooling gas, and 1.2 L min^{-1} for nebulizer gas. Sample and skimmer cones of nickel were installed with a 4.5 mm robust insert to increase matrix tolerance for seawater. The ICP-MS was operated in helium kinetic energy discrimination (He KED) mode with a Qcell collision/reaction gas flowrate of 5 mL min^{-1}. Na and Cl standard solutions were prepared for a concentration range from 0.1 ppm to 5 ppm using serial dilution of a NaCl standard (Ricca Chemical). Pt (Sigma Aldrich), Ir (Ricca Chemical), and Fe (Sigma Aldrich) standard solutions were prepared for a concentration range from 0 ppb to 100 ppb using serial dilution. All measurements were performed with three repetitions of ten sweeps using a 100 ms dwell time and reported error bars correspond to the relative standard deviation (on average, ~5% RSD).

Three-Electrode Measurements

The three electrode measurements (**Figure S12**) designed to evaluate Cl^- electrooxidation were executed using the appropriate PTL with catalyst and ionomer overlayer (e.g. stainless steel with IrO_x and PiperION to simulate a BPMWE anode; Pt/Ti with IrO_x and Nafion simulate a PEMWE anode) as a working electrode in aqueous 0.5 M H_2SO_4 or 1 M NaOH with 0.5 M NaCl electrolytes to mimic the interface pH environment of PEMWE or BPMWE, respectively. Counter electrodes in all cases were the same catalyst and ionomer coated carbon paper electrodes as were also used in the electrolyzer configuration and were separated from the working electrode by a Nafion membrane. Ag/AgCl reference electrodes were placed in the working electrode compartment of the Teflon H-cell to monitor working and counter electrode potentials. Electrolysis was performed both at a range of constant potentials near the onset of COR as well as at two current densities of relevance to this work (i.e. 100 mA cm^{-2} and 250 mA cm^{-2}).

Chloride Oxidation Quantification

Cl^- oxidation to free chlorine was quantified using a commercially available colorimetric 'DPD' test (Thermo Scientific Orion™ Chlorine Free-DPD Powder Packs; DPD = , N-diethyl-p-phenylenediamine). Briefly, the contents of one as-received 'DPD Powder Pack' were added to a 10 mL analyte solution in a sealable vial. The vial was shaken vigorously for 10 seconds. A vibrant pink color would develop if free chlorine was present in the aliquot. Immediately after adding DPD, the sample was placed into a disposable polystyrene UV-Vis cuvette with a path length of 1 cm. The UV-Vis spectrometer (Agilent Cary 6000i) was configured in double beam mode with DI water in the reference cuvette and scanned at 10 nm/sec from 800 nm to 200 nm. Background scans were acquired by adding a DPD packet to DI water. To quantify free chlorine concentrations, absorbance was recorded at 552 nm. 552 nm is the wavelength of maximum absorbance of DPD when it has been oxidized by any free chlorine species to generate its "Wurster Dye" radical analogue.[45,46] This absorbance was then converted to a free chlorine concentration according to an established calibration curve (**Figure S23)**. To account for potential free chlorine degradation with time, we measured the rate of free chlorine concentration decrease in solutions that were flowed through a BPM and PEM electrolyzers under **1)** open circuit conditions, **2)** electrolysis conditions at 500 mA cm^{-2}, and **3)** two different anode PTL compositions (**Figure S11)**. The rate of degradation in all cases was sufficiently slow on the time scale of our experiments as to be considered negligible.

X-Ray Photoelectron Spectroscopy

Electrode surface composition was analyzed with a Phi VersaProbe 3 with monochromatized Al (Kα) radiation, 200 μm spot size, 50 W power, and 15 kV gun voltage. Samples were neutralized during acquisition with an electron flood gun and an Ar ion gun and spectral signatures were identified according to their binding energies relative to adventitious carbon signal at 284.8 eV.

Scanning Electron Microscopy

Electrode morphology was observed with a Thermo Fisher Scientific Apreo S LoVac Scanning Electron Microscope with Trinity detector system and NiCol electron column under high-vacuum conditions with an accelerating voltage of 15 kV (~1.0 nm beam resolution), a 10 pA beam current and a working distance of 10 mm. Scale bars were generated from pixel-calibrated image files in ImageJ software.

SUPPLEMENTAL INFORMATION

Document S1. Calculations, Supplemental Discussion, Supplemental Experimental Procedures, Figures S1–S16.

ACKNOWLEDGMENTS

Primary funding was provided by the U.S. Office of Naval Research under grant N00014-20-1-2517. Partial support for long-term seawater durability measurements was provided by the Stanford Doerr School of Sustainability Accelerator. Partial support for ICP-MS measurements and COR three-electrode measurements was provided by the U.S. Department of Energy, Office of Science, Office of Basic Energy Sciences, Chemical Sciences, Geosciences, and Biosciences Division, Catalysis Science Program through the SUNCAT Center for Interface Science and Catalysis. Partial support for GAL and some electrode development was provided by the U.S. Department of Energy Office of Energy Efficiency and Renewable Energy (EERE)

Fuel Cell Technologies Office (FCTO) Award DE-EE0008841. GAK and VAN were supported by the National Science Foundation Graduate Research Fellowship Grant No. 1650114. DHM was supported by a National GEM Consortium GEM Fellowship and a TomKat Center for Sustainable Energy Fellowship for Translational Research.

Part of this work was performed at the Stanford Nano Shared Facilities (SNSF) supported by the National Science Foundation under award ECCS-2026822.

AUTHOR CONTRIBUTIONS

Conceptualization: DHM, JTP, MAH, GAL, LC, MBS ACN, SWB, TFJ
Methodology: DHM, JTP, MAH, AMA, GAK, VAN, YNR, ACN
Investigation: DHM, JTP, MAH, AMA, GAK, VAN, ACN
Visualization: DHM, JTP
Funding acquisition: SWB, TFJ, MAH, ACN
Project administration: SWB, ACN, TFJ
Supervision: SWB, TFJ, ACN
Writing – original draft: DHM, JTP
Writing – review & editing: DHM, JTP, MAH, GAL, LC, GAK, MBS, YNR, SWB, CAN, TFJ

DECLARATION OF INTERESTS

The authors have patents submitted and issued (US patent # 11,268,200) related to the content of this manuscript.

INCLUSION AND DIVERSITY

One or more of the authors in this paper self-identifies as an underrepresented ethnic minority in their field of research or within their geographical location. One or more of the authors in this paper self-identifies as a gender minority in their research field. One or more of the authors in this paper received support from a program designed to increase minority representation in their field of research.

REFERENCES*

1. Gao, F.-Y., Yu, P.-C., and Gao, M.-R. (2022). Seawater electrolysis technologies for green hydrogen production: challenges and opportunities. Current Opinion in Chemical Engineering *36*, 100827. 10.1016/j.coche.2022.100827 .

2. Caldera, U., and Breyer, C. (2017). Learning curve for seawater reverse osmosis desalination plants: Capital cost trend of the past, present, and future. Water Resour. Res. *53*, 10523–10538. 10.1002/2017WR021402.

3. Farràs, P., Strasser, P., and Cowan, A.J. (2021). Water electrolysis: Direct from the sea or not to be? Joule *5*, 1921–1923. 10.1016/j.joule.2021.07.014.

4. Gao, L., Yoshikawa, S., Iseri, Y., Fujimori, S., and Kanae, S. (2017). An economic assessment of the global potential for seawater desalination to 2050. Water *9*, 763. 10.3390/w9100763.

5. Wang, S., Liu, H., Gu, J., Sun, H., Zhang, M., and Liu, Y. (2019). Technology feasibility and economic viability of an innovative integrated ceramic membrane bioreactor and reverse osmosis process for producing ultrapure water from municipal wastewater. Chemical Engineering Journal *375*, 122078. 10.1016/j.cej.2019.122078.

6. Azinheira, G., Segurado, R., and Costa, M. (2019). Is renewable energy-powered desalination a viable solution for water stressed regions? A case study in Algarve, Portugal. Energies *12*, 4651. 10.3390/en12244651.

7. O'Brien, T., Bommaraju, T.V., and Hine, F. (2005). Handbook of Chlor-Alkali Technology (Springer).

8. Kirk, D., and Ledas, A. (1982). Precipitate formation during sea water electrolysis. International Journal of Hydrogen Energy *7*, 925–932. 10.1016/0360-3199(82)90160-4.

9. Dresp, S., Dionigi, F., Klingenhof, M., and Strasser, P. (2019). Direct electrolytic splitting of seawater: Opportunities and challenges. ACS Energy Lett. *4*, 933–942. 10.1021/acsenergylett.9b00220.

10. Lindquist, G.A., Xu, Q., Oener, S.Z., and Boettcher, S.W.

(2020). Membrane electrolyzers for impure-water splitting. Joule *4*, 2549–2561. 10.1016/j.joule.2020.09.020.

11. Millet, P., Ranjbari, A., de Guglielmo, F., Grigoriev, S.A., and Auprêtre, F. (2012). Cell failure mechanisms in PEM water electrolyzers. International Journal of Hydrogen Energy *37*, 17478–17487. 10.1016/j.ijhydene.2012.06.017.

12. Dresp, S., Ngo Thanh, T., Klingenhof, M., Brückner, S., Hauke, P., and Strasser, P. (2020). Efficient direct seawater electrolysers using selective alkaline NiFe-LDH as OER catalyst in asymmetric electrolyte feeds. Energy Environ. Sci. *13*, 1725–1729. 10.1039/D0EE01125H.

13. Veroneau, S.S., and Nocera, D.G. (2021). Continuous electrochemical water splitting from natural water sources via forward osmosis. Proc. Natl. Acad. Sci. U.S.A. *118*, e2024855118. 10.1073/pnas.2024855118.

14. Han, J.-H., Jwa, E., Lee, H., Kim, E.J., Nam, J.-Y., Hwang, K.S., Jeong, N., Choi, J., Kim, H., Jeung, Y.-C., et al. (2022). Direct seawater electrolysis via synergistic acidification by inorganic precipitation and proton flux from bipolar membrane. Chemical Engineering Journal *429*, 132383. 10.1016/j.cej.2021.132383.

15. Han, J. (2022). Exploring the Interface of Porous Cathode/Bipolar Membrane for Mitigation of Inorganic Precipitates in Direct Seawater Electrolysis. ChemSusChem *15*. 10.1002/cssc.202200372.

16. Consonni, V., Trasatti, S., Pollak, F., and O'Grady, W.E. (1987). Mechanism of chlorine evolution on oxide anodes study of pH effects. J. Electroanal. Chem *228*, 393–406. 10.1016/0022-0728(87)80119-5.

17. Dionigi, F., Reier, T., Pawolek, Z., Gliech, M., and Strasser, P. (2016). Design criteria, operating conditions, and nickel–iron hydroxide catalyst materials for selective seawater electrolysis. ChemSusChem *9*, 962–972. 10.1002/cssc.201501581.

18. Vos, J.G., Liu, Z., Speck, F.D., Perini, N., Fu, W., Cherevko, S., and Koper, M.T.M. (2019). Selectivity trends between oxygen evolution and chlorine evolution on iridium-based double perovskites in acidic media. ACS Catal. *9*, 8561–8574. 10.1021/acscatal.9b01159.

19. McCrory, C.C.L., Jung, S., Peters, J.C., and Jaramillo, T.F. (2013). Benchmarking heterogeneous electrocatalysts for the oxygen evolution reaction. J. Am. Chem. Soc. *135*, 16977–16987. 10.1021/ja407115p.

20. Vos, J.G., Wezendonk, T.A., Jeremiasse, A.W., and Koper, M.T.M. (2018). MnOx/IrOx as Selective Oxygen Evolution Electrocatalyst in Acidic Chloride Solution. J. Am. Chem. Soc. *140*, 10270–10281. 10.1021/jacs.8b05382.

21. Pourbaix, M. (1974). Atlas of Electrochemical Equilibria in Aqueous Solution.

22. Berlinger, S.A., McCloskey, B.D., and Weber, A.Z. (2018). Inherent acidity of perfluorosulfonic acid ionomer dispersions and implications for ink aggregation. J. Phys. Chem. B *122*, 7790–7796. 10.1021/acs.jpcb.8b06493.

23. Wang, J., Zhao, Y., Setzler, B.P., Rojas-Carbonell, S., Ben Yehuda, C., Amel, A., Page, M., Wang, L., Hu, K., Shi, L., et al. (2019). Poly(aryl piperidinium) membranes and ionomers for hydroxide exchange membrane fuel cells. Nat Energy *4*, 392–398. 10.1038/s41560-019-0372-8.

24. Vermaas, D.A., and Smith, W.A. (2016). Synergistic electrochemical CO_2 reduction and water oxidation with a bipolar membrane. ACS Energy Lett. *1*, 1143–1148. 10.1021/acsenergylett.6b00557.

25. Dickson, A.G., and Goyet, C. (1994). Handbook of Methods for the Analysis of the Various Parameters of the Carbon Dioxide System in Sea Water. Version 2 (Oak Ridge National Lab., TN (United States)).

26. Oener, S.Z., Foster, M.J., and Boettcher, S.W. (2020). Accelerating water dissociation in bipolar membranes and for electrocatalysis. Science *369*, 1099–1103. 10.1126/science.aaz1487.

27. Chen, L., Xu, Q., Oener, S.Z., Fabrizio, K., and Boettcher, S.W. (2022). Design principles for water dissociation catalysts in high-performance bipolar membranes. Nat Commun *13*, 3846. 10.1038/s41467-022-31429-7.

28. Pintauro, P.N., and Bennion, D.N. (1984). Mass transport of electrolytes in membranes. 2. Determination of sodium chloride equilibrium and

transport parameters for Nafion. Ind. Eng. Chem. Fundam *23*, 234–243. 10.1021/i100014a017.

29. Khalid, H., Najibah, M., Park, H.S., Bae, C., and Henkensmeier, D. (2022). Properties of anion exchange membranes with a focus on water electrolysis. Membranes *12*, 989. 10.3390/membranes12100989.

30. Li, D., R. Motz, A., Bae, C., Fujimoto, C., Yang, G., Zhang, F.-Y., E. Ayers, K., and Seung Kim, Y. (2021). Durability of anion exchange membrane water electrolyzers. Energy Environ. Sci *14*, 3393–3419. 10.1039/D0EE04086J.

31. Dickinson, E.J.F., Limon-Petersen, J.G., and Compton, R.G. (2011). The electroneutrality approximation in electrochemistry. J Solid State Electrochem *15*, 1335–1345. 10.1007/s10008-011-1323-x.

32. Gao, K.W., Yu, X., Darling, R.M., Newman, J., and Balsara, N.P. (2022). Increased Donnan exclusion in charged polymer networks at high salt concentrations. Soft Matter *18*, 282–292. 10.1039/D1SM01511G.

33. Blommaert, M.A., Verdonk, J.A.H., Blommaert, H.C.B., Smith, W.A., and Vermaas, D.A. (2020). Reduced ion crossover in bipolar membrane electrolysis via increased current density, molecular size, and valence. ACS Appl. Energy Mater. *3*, 5804–5812. 10.1021/acsaem.0c00687.

34. Bui, J.C., Digdaya, I., Xiang, C., Bell, A.T., and Weber, A.Z. (2020). Understanding multi-ion transport mechanisms in bipolar membranes. ACS Appl. Mater. Interfaces *12*, 52509–52526. 10.1021/acsami.0c12686.

35. Paddison, S.J., and Paul, R. (2002). The nature of proton transport in fully hydrated Nafion®. Phys. Chem. Chem. Phys. *4*, 1158–1163. 10.1039/b109792j.

36. Adam, L.C., and Gordon, G. (1999). Hypochlorite ion decomposition: Effects of temperature, ionic strength, and chloride ion. Inorg. Chem. *38*, 1299–1304. 10.1021/ic980020q.

37. Lindquist, G.A., Oener, S.Z., Krivina, R., Motz, A.R., Keane, A., Capuano, C., Ayers, K.E., and Boettcher, S.W. (2021). Performance and durability of pure-water-fed anion exchange membrane electrolyzers using baseline materials and operation. ACS Appl. Mater. Interfaces *13*, 51917–51924. 10.1021/acsami.1c06053.

38. Krivina, R.A., Lindquist, G.A., Beaudoin, S.R., Stovall, T.N., Thompson, W.L., Twight, L.P., Marsh, D., Grzyb, J., Fabrizio, K., Hutchison, J.E., et al. (2022). Anode catalysts in anion-exchange-membrane electrolysis without supporting electrolyte: Conductivity, dynamics, and ionomer degradation. Adv. Mater *34*, 2203033. 10.1002/adma.202203033.

39. Rossi, R., Hall, D.M., Shi, L., Cross, N.R., Gorski, C.A., Hickner, M.A., and Logan, B.E. (2021). Using a vapor-fed anode and saline catholyte to manage ion transport in a proton exchange membrane electrolyzer. Energy Environ. Sci. *14*, 6041–6049. 10.1039/D1EE02265B.

40. Bernt, M., Hartig-Weiß, A., Tovini, M.F., El-Sayed, H.A., Schramm, C., Schröter, J., Gebauer, C., and Gasteiger, H.A. (2020). Current challenges in catalyst development for PEM water electrolyzers. Chem. Ing. Tech. *92*, 31–39. 10.1002/cite.201900101.

41. Sun, S., Shao, Z., Yu, H., Li, G., and Yi, B. (2014). Investigations on degradation of the long-term proton exchange membrane water electrolysis stack. Journal of Power Sources *267*, 515–520. 10.1016/j.jpowsour.2014.05.117.

42. Green hydrogen cost reduction: Scaling up electrolysers to meet the 1.5°C climate goal (2020). (International Renewable Energy Agency (IRENA)).

43. Suermann, M., Bensmann, B., and Hanke-Rauschenbach, R. (2019). Degradation of proton exchange membrane (PEM) water electrolysis cells: Looking beyond the cell voltage increase. J. Electrochem. Soc. *166*, F645–F652. 10.1149/2.1451910jes.

44. Mayyas, A.T., Ruth, M.F., Pivovar, B.S., Bender, G., and Wipke, K.B. (2019). Manufacturing cost analysis for proton exchange membrane water electrolyzers 10.2172/1557965.

45. 4500-Cl CHLORINE (RESIDUAL) Standard Methods For the Examination of Water and Wastewater.

46. Tarvin, D., Todd, H.R., and Buswell, A.M. (1934). The Determination of Free Chlorine. Journal - American Water Works Association *26*, 1645–1662. 10.1002/j.1551-8833.1934.tb14393.x.

REFERENCES*

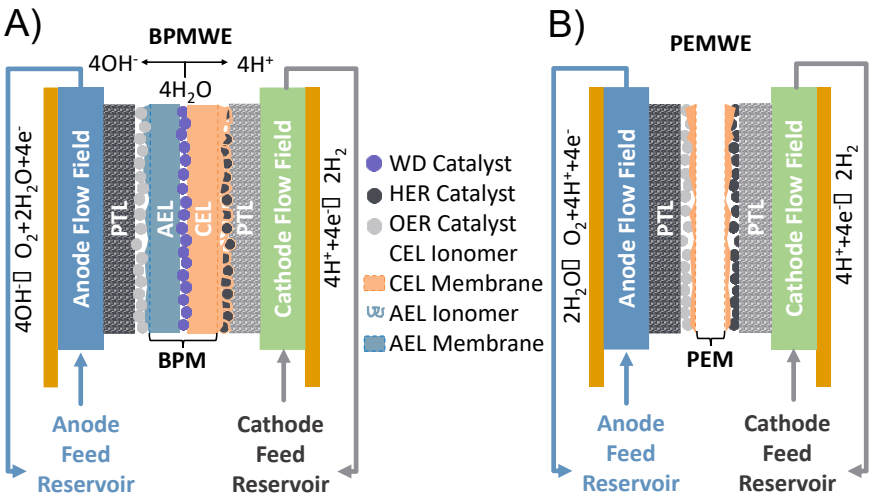

Figure 1. BPMWE and PEMWE device schematics

A) Cross-sectional schematic of a zero-gap BPMWE, and **B)** cross-sectional schematic of a zero-gap PEMWE, illustrating the positioning of catalyst/ionomer-coated porous transport layers relative to their respective ion-exchange membranes, as well as the circulation scheme that was used for all electrolyzer experiments. Reservoirs were heated to 60 °C, resulting in a measured temperature of 50 °C at the electrolyzer body (see SI). Schematics are not drawn to scale. In these electrolyzers, CEL is defined as being the Nafion membrane as well as the Nafion ionomer of the catalyst layer(s), while AEL is defined as being the PiperION membrane and the PiperION ionomer of the catalyst layer.

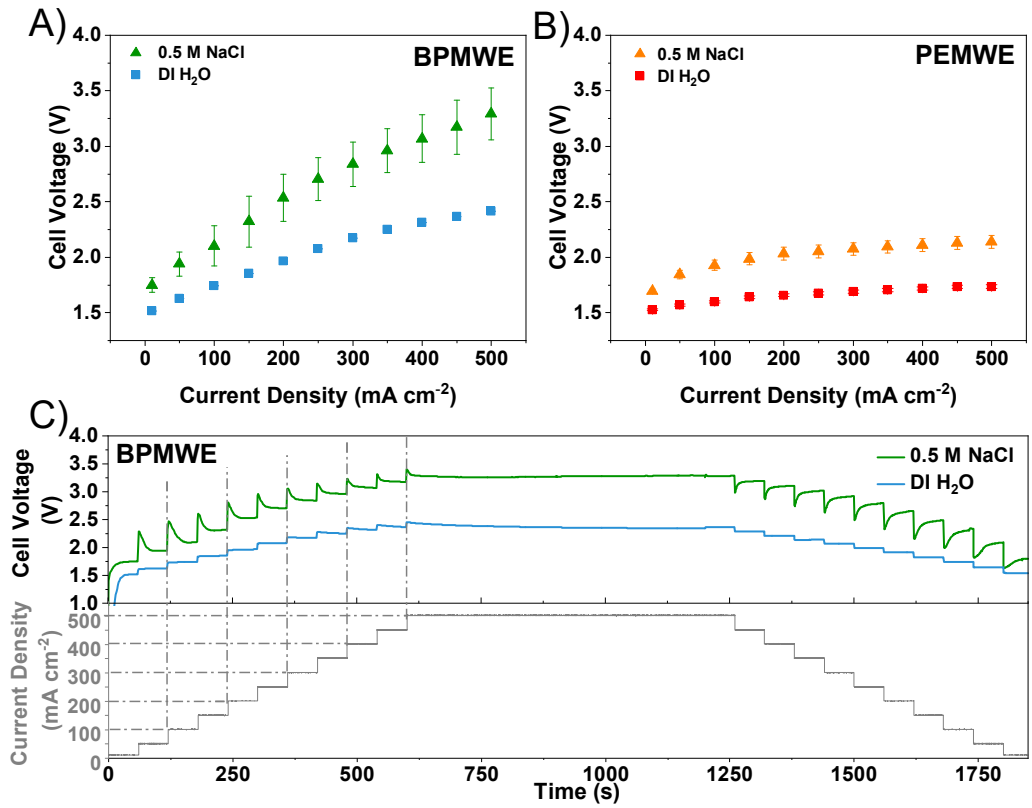

Figure 2. Characterization of device performance in deionized water and in 0.5 M NaCl

A, B) Polarization curves with 0.5 M $NaCl_{aq}$ (**green, orange triangles**) as the cathode feed compared to with DI H_2O (**blue, red squares**) as the cathode feed in a BPMWE **(A)** and a PEMWE **(B). C)** Voltage vs. time during stepped chronopotentiometry with (**green**) and without (**blue**) 0.5 M $NaCl_{aq}$ in a BPM electrolyzer cathode feed. On the lower y-axis, the grey trace is the corresponding applied current density profile during stepped chronopotentiometry. Error bars in all cases represent a single standard deviation extracted from no less than three replicate experiments.

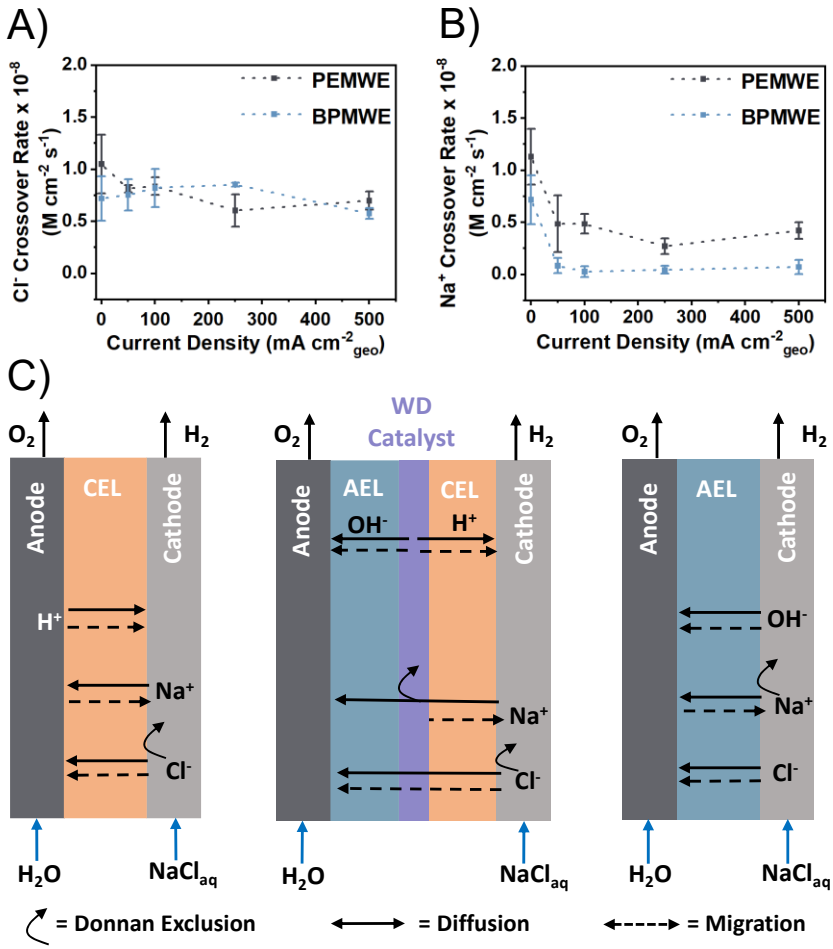

Figure 3. Ion transport dynamics in membrane electrolyzers

A) Cl^- crossover rates with increasing applied current density, and **B)** Na^+ crossover rates with increasing applied current density for BPMWE (**blue**) versus PEMWE (**gray**). Error bars in all cases represent standard deviations from triplicated experimental data. These rates are described as molar fluxes defined with units of M cm^{-2} s^{-1}. We note that both cathode and anode chamber contained 1 L of solution, enabling the ready conversion these units to mol cm^{-2} s^{-1}. Connecting lines are guides for data interpretation. **C)** Proposed key ion transport effects for PEMWE (**left**), BPMWE (**middle**), and AEMWE (**right**), including diffusion (solid arrows), migration (dashed arrows) and Donnan exclusion effects (curved arrows) that dictate transport of ions across the ion-exchange membranes.

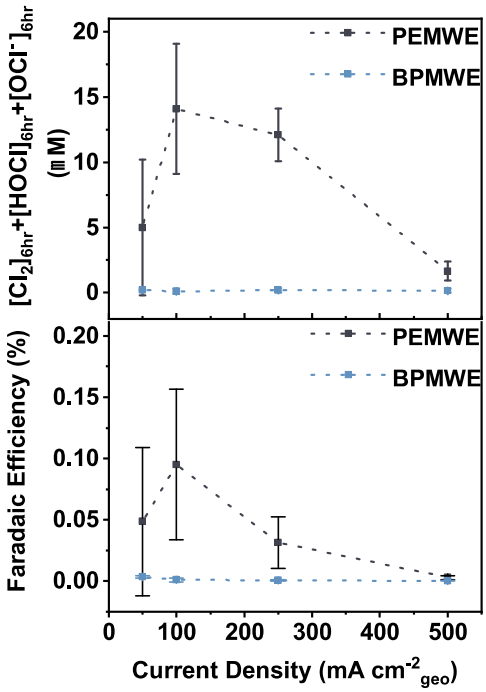

Figure 4. Chloride electrooxidation behavior

BPMWE (**blue**) and PEMWE (**gray**) free chlorine concentrations after 6 h of 0.5 M $NaCl_{aq}$ electrolysis (**top**) and Faradaic efficiency for Cl^- oxidation to free chlorine (**bottom**). Error bars are single standard deviations from triplicate experiments.

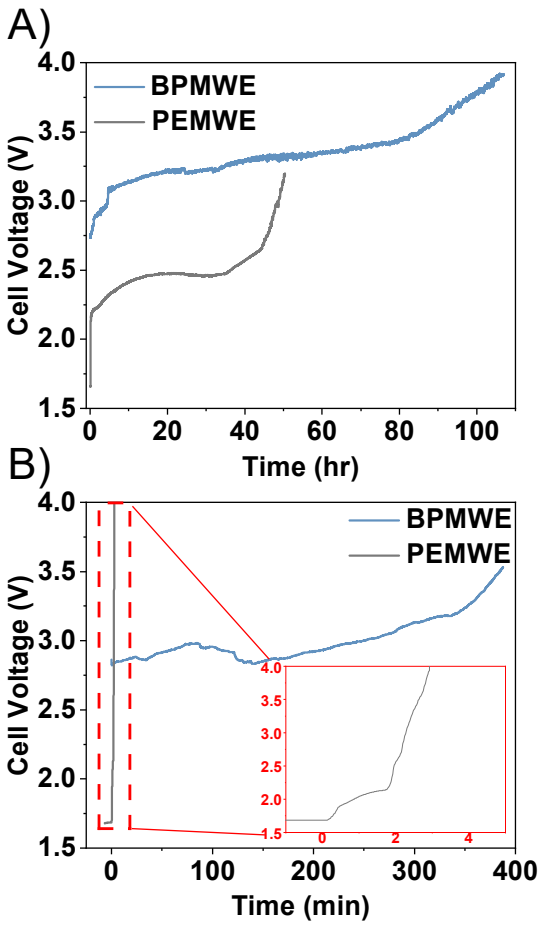

Figure 5. Device stability during real seawater electrolysis

V-t behavior during chronopotentiometry for a BPMWE (**blue**) and a PEMWE (**grey**) at a fixed current of 250 mA cm^{-2} **A)** with seawater as the cathode feed and DI water as the anode feed, and **B)** with seawater fed to both cathode and anode. Inset highlights the entirety of the PEMWE experiment where immediate failure was observed. The first voltage increase at t = 0 min coincides with exchanging the cathode feed for seawater and the second voltage increase ~2 min coincides with exchanging the anode feed for seawater.

Table 1. Total cell voltages required to drive PEMWE and BPMWE devices at various applied current densities under DI-water fed conditions and asymmetric 0.5 M $NaCl_{aq}$ fed conditions.

	DI water j = 50 mA cm^{-2}	DI water j = 500 mA cm^{-2}	0.5 M $NaCl_{aq}$ j = 50 mA cm^{-2}	0.5 M $NaCl_{aq}$ j = 500 mA cm^{-2}	ΔV_{Cell} j = 500 mA cm^{-2} (V_{NaCl} -V_{DI})
V_{cell} PEMWE (V)	1.57 ± 0.01	1.73 ± 0.02	1.84 ± 0.04	2.14 ± 0.06	0.41 ± 0.06
V_{cell} BPMWE (V)	1.63 ± 0.02	2.4 ± 0.2	1.94 ± 0.07	3.3 ± 0.2	0.9 ± 0.3